High-resolution angle-resolved positron reemission spectra from metal surfaces

D. A. Fischer* and K. G. Lynn
Physics Department, Brookhaven National Laboratory, Upton, New York 11973

D. W. Gidley
Physics Department, The University of Michigan, Ann Arbor, Michigan 48109
(Received 11 October 1985)

An electrostatically focused beam of monoenergetic positrons is used with a hemispherical energy analyzer to acquire the first high-resolution ($\approx$20 meV) total-energy spectra of positrons reemitted from metal single crystals. At 300 K the measured energy width of positrons elastically emitted (with kinetic energy corresponding to the magnitude of the negative positron work function) is $\approx 75\pm5$ meV for all the samples investigated: Ni(100), Ni(100)+CO, Ni(100)+S, Ni(100)+O, W(110)+C, W(110)+Cu, W(110)+O, Cu(111), Cu(111)+S, and Cu(100)+S. These results, along with angular distribution measurements on W(110)+C, W(110)+O, and Cu(111), are completely consistent with energy and angular widths as determined by a beam Maxwell-Boltzmann distribution—i.e., thermal broadening alone. A much narrower peak is observed at sample temperatures of 23 K, but uncertainty in the analyzer resolution limits us to conclude that the observed broadening is consistent with a thermal distribution with effective temperature less than 100 K. Discrete energy-loss peaks due to vibrational excitations of adsorbed molecules on the sample surface, first reported by Fischer *et al.* [Phys. Rev. Lett. **50**, 1149 (1983)], are further investigated for Ni(100)$c(2\times2)$/CO. The first evidence for short-range positron "impact" scattering is found for OH adsorbed on NiO as a loss peak at 400 meV in the reemitted spectrum. Continuous inelastic scattering processes are also observed in the spectrum and a limit on wide-angle elastic scattering is determined from angular scans. A discussion comparing electron-energy-loss spectroscopy with positron-energy-loss spectroscopy is presented along with a brief discussion of possible improvements to positron-energy-loss spectroscopy, including the use of brightness-enhanced beams, spin-polarized positron beams, and liquid-helium-cooled samples for narrow-energy-width beams.

I. INTRODUCTION

Since the discovery that thermalized positrons in many metals exhibit a negative work function,[1-3] experiments have studied various aspects of the positron-emission process.[4-6] This direct positron-emission process has been compared to that for negative electron affinity systems and appears to have some similar characteristics,[7] i.e., narrow angular distribution and small energy spread. However, the studies of positron emission are motivated by the rich variety of interactions the positron can undergo at the surface of a metal, including direct emission into the vacuum (measurement of the positron work function), continuous inelastic processes such as electron-hole pair excitation, discrete energy loss to adsorbed molecules,[8] localization in a surface image-correlation well,[5] penetration through and thermalization in epitaxially grown overlayers,[9,10] and even surface electron capture to form the bound-state positronium. In this paper we will present a detailed study of two aspects of positron-emission spectroscopy: the total-energy spectrum and the angular distribution of positrons emitted from well-characterized metal surfaces. Using Ni, W, and Cu surfaces we report high-resolution total-energy[11] ($\Delta E\simeq20$ meV) emission spectra for both room-temperature and 23-K single-crystal samples. Finally, we present more-detailed results of an experiment[8] that demonstrated the feasibility of positron energy-loss spectroscopy as a surface probe by measuring the discrete energy loss of positrons to vibrational excitation of adsorbed molecules.

The organization of this paper is as follows. In Sec. II the experimental apparatus and procedures are described. In Sec. III we discuss the elastic emission processes as well as information ascertained from elastic emission concerning the interaction of the positron with the bulk sample. Also included are a discussion of thermalization and apparent effective mass in the sample, and measurements of the positron-emission angles. In Secs. IV and V we will present data and a simple theory of inelastic energy loss at the surface for both discrete and continuous processes (i.e., dipole and impact scattering and electron-hole excitation). Section VI contains concluding remarks as well as a discussion of the relative merits of electron and positron energy-loss measurements.

II. EXPERIMENTAL ANALYZER DESIGN CONSIDERATIONS FOR REEMITTED-POSITRON ENERGY-LOSS SPECTROSCOPY (REPELS)

In order to measure a REPELS spectrum one would like a differential energy analyzer with good angle resolution (1° or 2°) and energy resolution (<10 meV). A

cylindrical mirror analyzer (CMA) or hemispherical analyzer would seem the logical choice.[12] A hemispherical analyzer has perfect source focusing in one angle (β, perpendicular to the plane of α in Fig. 1) and first-order focusing in the other, α.[12] On the other hand, a CMA has the advantage of second-order focusing in α at the "magic" angle ($\alpha=42°\ 18.5'$). However, the polar angles α and β are coupled (whereas in the hemispherical analyzer they are not) thus requiring the sample normal to be tilted by the magic angle with respect to the CMA axis. The requirement, coupled with the geometrical constraints of our surface chamber, necessitated the use of the hemispherical analyzer in our experiment.

For a hemispherical analyzer the pass energy of the central ray is given by (see Fig. 1)

$$E_0=c\Delta Vq\ , \tag{1}$$

where $c=r_1r_2/(r_2^2-r_1^2)$. The analyzer used in the REPELS experiments has $r_1=1.187$ in., $r_2=1.687$ in. making $c=1.394$; thus, for example, a potential difference across the analyzer spheres of 1.0 V results in a positron central energy (pass energy) of 1.394 eV. The resolution of a hemispherical analyzer is given by[12] (see Fig. 1)

$$\frac{\Delta E}{E_0}=\frac{x_1}{2\bar{r}}+\frac{x_2}{2\bar{r}}+\alpha^2\ , \tag{2}$$

where x_1 and x_2 are the input and exit slit half-widths, respectively. Here $\bar{r}$ represents the central radius of the analyzer or the average of r_1 and r_2, and α is the half-angle of emission from the source.

If $x_1=x_2$ (equal input and output slits of full width w) then Eq. (2) becomes

$$\frac{\Delta E}{E_0}=\frac{w}{2\bar{r}}+\alpha^2\ . \tag{3}$$

According to Kuyatt and Simpson,[13] if $\alpha^2<w/2\bar{r}$ then aberrations at the exit aperture will be kept to a minimum.

A schematic diagram of the top view of the REPELS apparatus is shown in Fig. 2. The sample may be rotated in front of the analyzer which allows angular scans (in α) of the reemitted-positron beam from the sample. Scanning α sweeps the sample emittance cone through the angular acceptance window of the analyzer. The analyzer half-angle acceptance is $\alpha=\pm5°$ and $\beta=\pm20°$.

The operation of the analyzer for good angle and energy resolution depends critically on the proper magnetic shielding of the analyzer and sample. A magnetic field component B (in milligauss) perpendicular to the plane of dispersion will tend to change the trajectory of a positron of energy E_0 (eV), to a trajectory of radius R (cm),[14] where

$$B=3370E_0^{1/2}/R\ . \tag{4}$$

The deflection d (cm) in a path length L (cm) is then

$$d\simeq\frac{L^2}{2R}=\frac{L^2B}{6740E^{1/2}}\ . \tag{5}$$

Our analyzer has a $\approx$15-cm path length, thus if we wish to keep the deflection less than the slit width (0.11 cm) for a pass energy of 1 eV the magnetic field must be less than 3 mG. To eliminate strong magnetic fields (primarily the earth's field $\approx$500 mG) the analyzer and reverse-view low-energy electron-diffraction optics are housed in a double μ-metal (permeability $>70\,000$ G/Oe) shield shown in Fig. 2. The residual magnetic field inside the shielded region (near the analyzer) was measured with a Hall probe to be less than ±3 mG.

Electric fields inside the analyzer must be kept very uniform since the potential difference between the spheres determines the trajectory of the positron. The analyzer hemispheres are constructed from oxygen-free high-

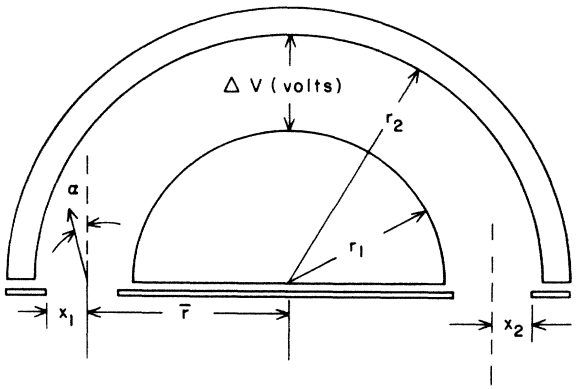

FIG. 1. Schematic drawing of a hemispherical electrostatic analyzer, r_1, r_2, $\bar{r}$, x_1, x_2, α, and ΔV are indicated; see text for definitions.

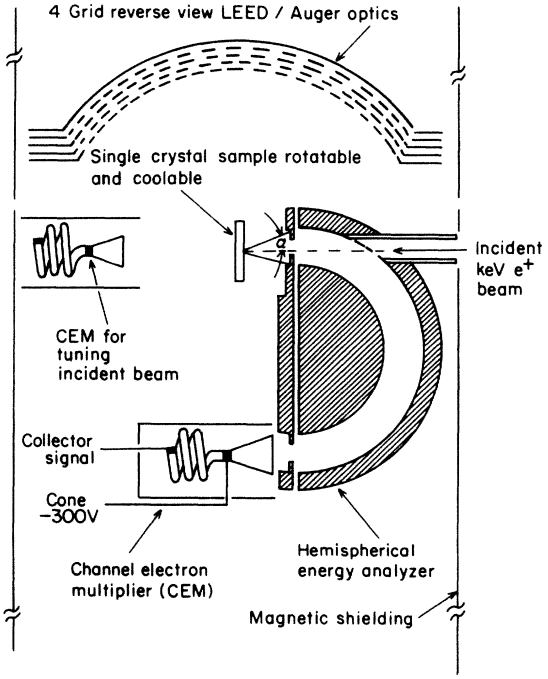

FIG. 2. Top view of the apparatus used for the measurement of reemitted-positron energy-loss spectroscopy. The analyzer, sample, and reverse-view LEED and Auger optics are contained in a double μ-metal shield to reduce magnetic fields.

conductivity copper,[15] and the incident-beam aperture in the outer hemisphere (Fig. 2) is covered with a 97%-transmitting Cu grid to maintain a uniform internal field. To reduce patch effects the inside of the analyzer was coated with graphite.[16] Baked graphite (350°C in vacuum) shows the smallest amount of patch effects[17] (nonuniformity of work function less than 10 meV). Patch effects and electric field uniformity were also found to be important in the region between the sample and the analyzer. For example, the contact potential [$(\Delta\phi^- \approx 0.6$ V) (Ref. 18)] between a tantalum screw holding a Cu(100) single crystal was found to change the trajectory of a nearby ($E < 1$ eV) positron reemitted from the copper crystal. These problems were minimized by using a large sample, keeping mounting hardware far from the regions of interest, and by using mounting hardware of the same material as the sample when feasible.

Positrons of several keV (with an energy spread of 1 eV or less) are incident on the sample through a hole in the outer hemisphere (see Fig. 2). A large fraction of the implanted positrons thermalize, diffuse to the surface, and are reemitted towards the input aperture of the analyzer. The reemitted positrons transmitted by the analyzer are counted by a channel electron multiplier (CEM) and accumulated as counts in a multichannel scalar as a function of the sample-to-analyzer voltage (positron retarding energy). The data are taken at a constant pass energy [E_0 in Eq. (1)]. This implies a constant energy resolution $\Delta E/E_0$ as defined by Eq. (3). The reemitted-positron energy distribution is accumulated by sweeping the analyzer's differential energy window ΔE through the REPELS spectrum by varying an applied potential between the sample and analyzer as shown in the Grotrian[19] diagram of Fig. 3.

The calculated analyzer resolution, ΔE, for our analyzer parameters (s is the sample-to-analyzer distance), $\bar{r} = 1.432$ in., $w = 0.044$ in.,

$$\alpha = \frac{w/2}{s} = \frac{0.022 \text{ in.}}{0.250 \text{ in.}} \simeq 0.009 ,$$

given by Eq. (3) is

$$\Delta E/E_0 = 0.023 .$$

For an incident energy distribution that is very narrow with respect to the analyzer resolution one would expect that a plot of the full width at half maximum, ΔE_{FWHM} (measured), versus the pass energy ideally to yield a straight line through the origin of slope 0.023. This was attempted experimentally by utilizing the positron-reemission spectrum from Ni(100) at 23 K, which was expected to have a ΔE_{FWHM} of ≈ 6 meV (for a directed Maxwell-Boltzmann distribution, see Sec. III). Figure 4 shows a plot of the measured ΔE_{FWHM} versus pass energy. For pass energies greater than 1.4 eV, where the inherent energy width of the emission spectrum is negligible, the points fall on a straight line of slope 0.030 yielding a resolution of $\Delta E/E_0 = 3.0\%$. This result is not inconsistent with our expectations since the calculation of α in Eq. (3) assumed a point source of positrons at the sample and, in fact, the source may be as large as the slit width itself. For this case we estimate that $\Delta E/E_0$ could be as large as ≈ 0.032, in reasonable agreement with the observed slope. For pass energies below 1.4 eV the plot in Fig. 4 departs from a straight line. At these low pass energies it is expected that patch effects and residual magnetic fields would limit the energy resolution of the analyzer. Extrapolating the observed ΔE_{FWHM} to zero pass energy, we deduce that the limiting analyzer resolution is about 20 meV (since we must deconvolve the inherent energy width of the cooled Ni sample as discussed

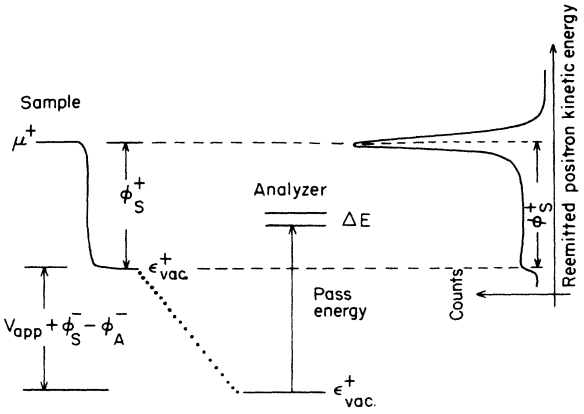

FIG. 3. Energy-level diagram showing how a measurement of the reemitted-positron energy distribution (REPELS) is made by sweeping an applied potential between the sample and analyzer.

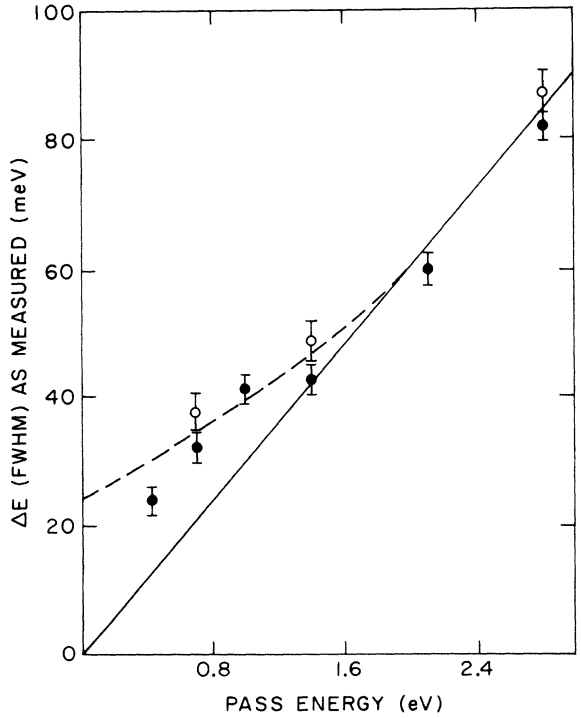

FIG. 4. Measured FWHM of the reemitted-positron elastic peak for Ni(100)$p(2\times2)$O at 23 K (solid circles) and clean Ni(100) (open circles) at 23 K is plotted versus pass energy. A hand-drawn line through the origin has been added whose slope is 0.030, yielding an analyzer resolution of $\Delta E_{\text{FWHM}}/E_0 = 3.0\%$.

in Sec. III). We note that when dealing with high-resolution electron-energy-loss monochromators and analyzers, one prefers to operate at pass energies greater than 1 eV where stray field effects are smaller and make resolution gains by employing narrow slits ($\Delta E/E_0 < 1\%$). However, in our case both the incident and reemitted-positron beams must pass through our analyzer entrance slit (see Fig. 2), and thus a comprise in slit width is required in order to maintain a high signal rate.

Sample cooling was accomplished by using a closed-cycle helium-gas refrigeration system. The sample temperature was measured using a Chromel-Alumel or tungsten-3% Re—tungsten-25% Re thermocouple for both low- and high-temperature measurements. At temperatures below 300 K measurements of the sample temperature were taken using an ice-point reference junction. After the experiments a precalibrated silicon thermometer[20] was varnished to the sample. The sample thermocouples were then calibrated to the silicon thermometer in liquid helium, helium vapor, and liquid nitrogen. We concluded that the sample temperature was about 23 ± 3 K when held by the thermal vise and after the helium refrigeration had been allowed to run 3 h to reach its equilibrium temperature.

All of the single-crystal samples were polished and etched prior to insertion in the vacuum system. The Ni(100) and Cu(111) samples were cleaned *in situ* by Ar^+-ion bombardment at 1-keV energy and heat treated at a temperature of 600 °C for $\approx$20 min.[21–23] After each sputtering—heat-treatment cycle, surface cleanliness was monitored using Auger electron spectroscopy (AES).[21–24] The W(110) sample was flashed to high temperatures ($\approx$2300 K) and subsequently heated in oxygen to remove the remaining carbon that was still present after the high-temperature flash. Even after these cycles were completed we found a small amount of carbon (0.1 monolayer) on the surface of the sample. The W(110) + O sample was produced by exposing the surface to 30 L of O_2 at 700 °C (1 L $=10^{-6}$ torr sec) and cooling. Special attention must be paid to the diffraction peaks found in the secondary-electron energy spectra during retarding-field Auger electron spectrscopy. These diffraction peaks can easily be mistaken for surface contamination and, in fact, indicate good surface order (see Ref. 23). Very sharp low-energy electron-diffraction (LEED) spots were observed after annealing in all of the samples studied. After annealing no sign of positron trapping at defects was detected in the experiment by measuring the variation of the yield of reemitted positrons versus incident positron energy.

III. THE ELASTIC PEAK

When positrons of several keV energy are implanted into a single-crystal target they rapidly lose energy and begin to approach thermal equilibrium in the lattice in $\approx 10^{-12}$ sec.[25] The kinetic energy of those positrons that diffuse back to the surface and are reemitted is measured with the hemispherical electrostatic energy analyzer. A large fraction of the reemitted positrons are contained in a peak in the energy spectrum, approximately 75 meV wide at room temperature, and with a mean energy corresponding to the magnitude of the positron work function ϕ^+. Although we will consider the possibility of wide-angle elastic scattering the angular distribution about the surface normal of elastic positrons is strongly peaked. We have concluded that the energy and angular distributions[26] of this elastic peak are consistent with thermal broadening.[8]

To demonstrate this assertion we must first ensure that the positrons reaching the surface have indeed thermalized with the bulk lattice. To ensure that this emission of nonthermal positrons is negligible, it is necessary to implant the incident positrons at a sufficiently high energy (i.e., deep enough below the surface). The effect of increasing beam energy is shown in Fig. 5 for Ni(100) + CO at room temperature. Unless otherwise specified the incident beam energy is 3 keV, the maximum available. We now estimate the broadening in energy and angle for elastically reemitted positrons due to thermal effects and compare these predictions with our measurements at 300 K and at 23 K for various target samples.

In our experiment the sample surface defines a plane that the thermalized diffusing positrons must cross to be reemitted, the hemispherical analyzer then defines a direction and solid angle of acceptance of the emitted beam. Thus if thermal positrons obey Maxwell-Boltzmann-like statistics, the reemitted beam should have a distribution of speeds similar to the *beam* Maxwell-Boltzmann distribution of speeds for molecules effusing from the collimated slit and oven of a molecular-beam apparatus. This argument assumes that the classical analog is correct for escaping Bloch-like positrons. The beam Maxwell-Boltzmann distribution of speeds $\Phi(v)dv$ gives the number of positrons (molecules) with speed in the range between v and $v+dv$ which emerge per unit time into a solid angle range $d\Omega$ from the sample surface (an oven with a small aperture in a side). It is given by

$$\Phi(v)dv \propto v^3 e^{-mv^2/2kT} dv\, d\Omega \ . \tag{6}$$

The beam Maxwell-Boltzmann distribution of speeds con-

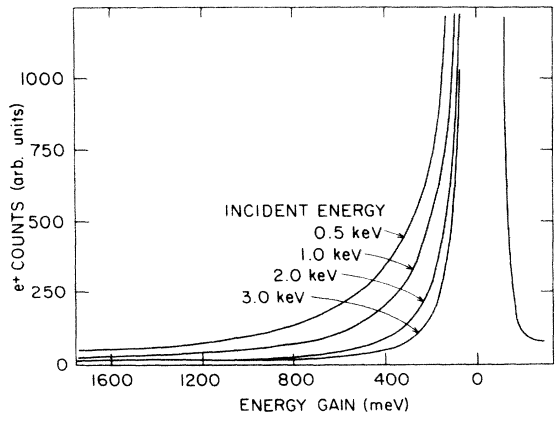

FIG. 5. Positron counts versus energy gain (above elastic peak energy) for a Ni(100) + CO sample at room temperature. The nonthermal tail is shown for a family of incident beam energies as indicated by arrows for 0.5, 1.0, 2.0, and 3.0 keV.

tains a factor v^3 rather than the factor v^2 for the Maxwell-Boltzmann speed distribution. This extra factor of v occurs because only positrons (molecules) a distance less than vdt from the sample surface (oven aperture), will cross the sample surface (oven aperture) in a time dt; therefore, faster positrons (molecules) have a greater probability of escape. Thus $\Phi(v)dv$ is the number of thermal positrons per unit time reemitted from the sample with speed between v and $v+dv$ into a solid angle $d\Omega$ normal to the sample. Since our analyzer measures kinetic energy we convert the distribution in Eq. (6) to one in energy, $F(E)dE$, the number of thermal positrons reemitted per unit time with energy E between E and $E+dE$ into a solid angle $d\Omega$,

$$F(E)dE \propto Ee^{-E/kT}dE\,d\Omega\ . \tag{7}$$

Typically a large fraction of the reemitted positrons are found to have a kinetic energy equal in magnitude to the positron work function, ϕ^+, and an energy spread (at 300 K) that is consistent with thermal broadening. The thermal broadening was confirmed in experiments[11] at low temperature where a narrowing of the elastic peak was observed for the first time as seen in Fig. 6 for a typical sample [Ni(100)]. The low-temperature elastic peak (and hence ϕ^+) is observed to be shifted to higher kinetic energy by 100 meV, a factor of 4 larger than the 25-meV increase observed for $\Delta\phi^-$.[27] We attribute this larger value to an enhanced sensitivity of positrons to contraction of the lattice which results in a more negative positron work function due to increased core repulsion, i.e., lattice contraction. A change in the surface dipole alone would not change the position of the elastic peak[26] where a change in μ^+ (positron chemical potential) relative to μ^- would produce the change. The elastic peaks shown in Fig. 6 show a tailing on the high-energy side of the peak which is a result of positrons that diffuse to the sample surface before complete thermalization.

The elastic peak shown in the REPELS spectrum may then be approximated by the convolution of a beam Maxwell-Boltzmann distribution of temperature T_{eff} with an assumed Gaussian analyzer resolution function of ΔE described in Sec. II. The theory was fitted to the data by minimizing the difference between the data and the convolution only over the full width at half maximum. This restricted fitting range was chosen to minimize the effects of the nonthermal positron tail. Figure 7 shows a representative fit for clean Ni(100) at room temperature (300 K) and low temperature (23 K). The 23 K peak is clearly much narrower and the effect of nonthermal positron tailing is more pronounced. The fitted curve at 23 K is nearly symmetric in shape because the convolution is dominated by the assumed Gaussian analyzer resolution. As a result of our lack of knowledge of the analyzer resolution the fit is relatively insensitive to T_{eff}. Table I shows a best fit of the convolution (explained above) for a variety of samples and pass energies at 23 and 300 K. As can be seen in Table I the range of acceptable fits for T_{eff} is $1 < T_{\text{eff}}/T < 5$ for $T = 23$ K. The upper limit is arrived at by assuming the smallest possible analyzer resolution—the value derived from the straight line in Fig. 4 (which is clearly an underestimate). Thus we can-

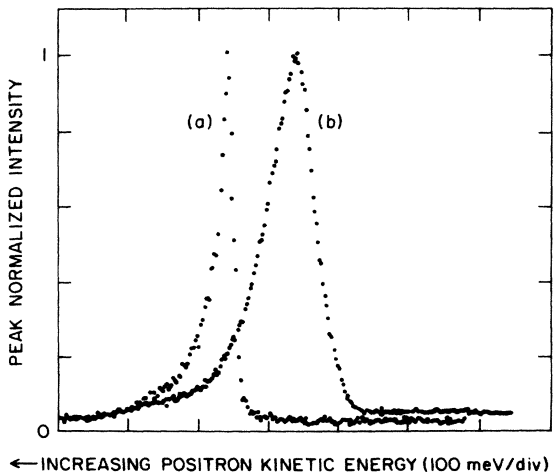

FIG. 6. Peak-normalized reemitted-positron intensity versus positron kinetic energy. Curve b is the elastic peak for Ni(100) at room temperature (300 K), curve a is at low temperature (23 K). The FWHM observed width of curve b is 80 meV and for curve a is 24 meV. The elastic peak counting rate is ≈ 5000 per sec, at 300 K.

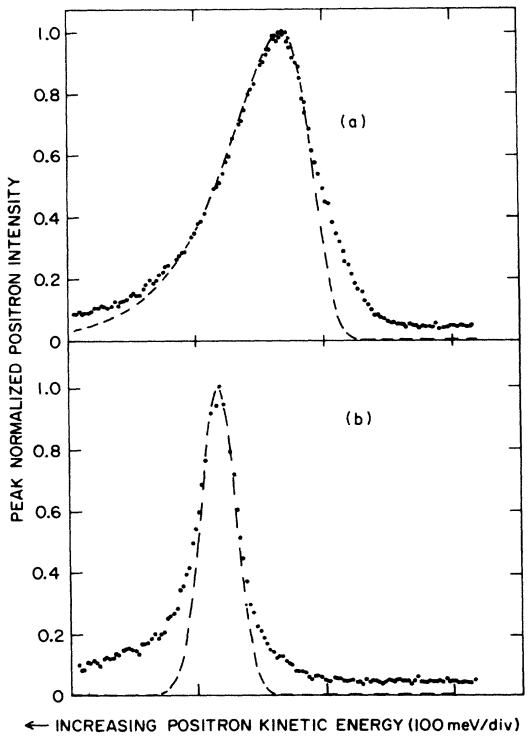

FIG. 7. (a) The as-recorded data for the elastic peak of clean Ni(100) at room temperature (dots) taken at a pass energy of 0.7 eV. On top of these data is a best fit (dashed curve) using the convolution of a beam Maxwell-Boltzmann energy distribution (T_{eff} from Table I) and a Gaussian analyzer resolution function (ΔE_{FWHM} from Table I). (b) Shows the elastic peak of clean Ni(100) at 23 K (dots) taken at a pass energy of 0.7 eV [same as Fig. 4(a)]. A best-fit convolution is shown (dashed curve) using T_{eff} and ΔE_{FWHM} from Table I.

TABLE I. A best fit was made to the reemitted-positron elastic peak data for a variety of samples and pass energies (as shown) at 23 and 300 K. The best fit is the convolution of a beam Maxwell-Boltzmann energy distribution of characteristic temperature T_{eff} and a Gaussian analyzer resolution function of width ΔE (meV). At 23 K we indicate the range of acceptable fits in the correlated parameters (ΔE, T_{eff}/T) determined on one hand by the lowest possible limit in ΔE and by $T_{\text{eff}}/T=1$ on the other.

	Pass energy		
Sample	1.4 eV	0.7 eV	0.42 eV
	Sample temperature ≃23 K		
Ni(100)$p(2\times2)$/O		25 meV, T	17 meV, T
		21 meV, $4T$	13 meV, $3T$
Ni(100)		30 meV, T	
		21 meV, $5T$	
Cu(111)	55 meV, T		
	42 meV, $5T$		
W(110) + 1.5 L of Cu	50 meV, T		
	42 meV, $4T$		
	Sample temperature ≃300 K		
Ni(100)		21 meV, $1.2T$	
Cu(111)		21 meV, $1.2T$	
W(110) + 1.5 L of Cu	42 meV, $0.8T$		

not rigorously conclude on the basis of our data that the reemission spectrum at 23 K is consistent with thermal broadening *only*. We note that these direct measurements of thermalization complement the angular correlation results of Kubica and Stewart,[28] which indicate that positrons thermalize in simple metals prior to annihilation at least as low as 77 K. However, at 4.2 K they[28] typically measured $T_{\text{eff}}=25\pm25$ K, a result not substantially different from our results, $T_{\text{eff}}<100$ K. Future reemission spectroscopy experiments with better (and more precisely measured) energy resolution and higher positron implantation energy are required.

At 300 K the fit to the data is largely insensitive to the analyzer resolution, and we simply quote the results of the best fit of the data, assuming the minimum analyzer resolution (3% of the pass energy). With $T_{\text{eff}}=1.2\pm0.1$, and given the relatively good fit of the convolution to the data in Fig. 7(a) (after allowance for a nonthermal tail on the gain side), we conclude that the elastic peak energy distribution for Ni, Cu, and W is consistent with thermal broadening alone. The possibility that the extra broadening in the wings of the energy-loss side in both Figs. 7(a) and 7(b) is due to electron-hole pair or phonon excitation inelastic processes is discussed in Sec. V.

In order to estimate the angular distribution we will, to a first approximation, consider the positron work function ϕ^+ merely to provide a one-dimensional potential step at the surface.[26] This will provide an additional energy in the z direction (normal to the crystal surface) of ϕ^+ resulting in an initial angular distribution of emitted positrons with a most probable half-angle of $\theta^i_{1/2}$. In addition, we will define $\theta^f_{1/2}$ to be the most probable half-angle after cutting the analyzer plane at a pass energy P:

$$\theta^i_{1/2}\simeq\left[\frac{E_{\text{prob}}}{\phi^+}\right]^{1/2}=\left[\frac{kT}{\phi^+}\right]^{1/2},$$
$$\theta^f_{1/2}\simeq\left[\frac{kT}{P}\right]^{1/2}, \tag{8}$$

where E_{prob} is the most probable energy of the positrons.

Angular scans in the angle α (see Fig. 2) with the analyzer tuned to the elastic peak, shown in Figs. 8 and 9, are performed by rotating the sample in 2° increments. In all scans the analyzer pass energy P was set to 1.4 eV, and thus it is necessary to account for the effect of the potential ($=\phi^+-P$) between the sample and analyzer. Assuming a uniform electric field, we calculate the effective angular spreading of positrons at the analyzer slit to be the average in reciprocal space of $\theta^i_{1/2}$ and $\theta^f_{1/2}$ [see Eq. (8)]. Thus,

$$\theta_{1/2}\approx\frac{2(E_{||})^{1/2}}{(\theta^+)^{1/2}+(P)^{1/2}}, \tag{9}$$

where $E_{||}=kT$ is 25 meV at 300 K. In Table II our calculations are compared with the measured FWHM from the scans. In addition, we have included a small ($\approx10\%$) correction to $\theta_{1/2}$ due to the distortion of the electric field when the sample is rotated (which effects $E_{||}$) before adding in quadrature with the $(4\pm1)°$ angular resolution of the analyzer. This half-angle is then doubled to yield θ_{FWHM}(calc) in the table.

It is clear from the 300-K data in Table II that the measured angular spreading is consistent with thermal broadening in the component of momentum parallel to

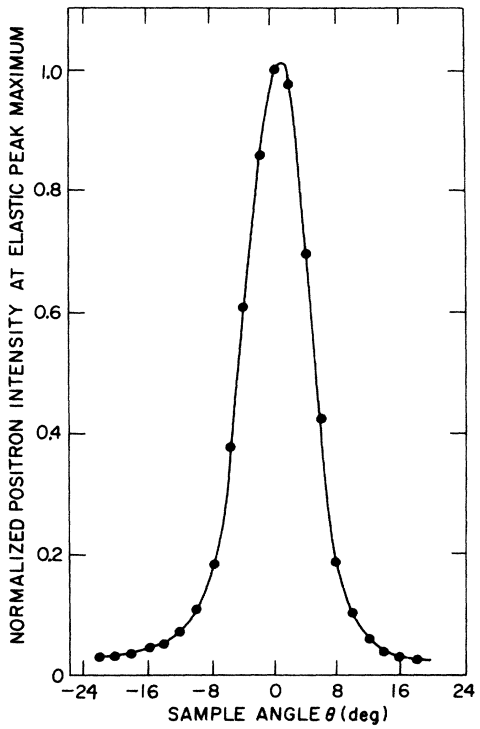

FIG. 8. Peak normalized positron counting rate for the analyzer tuned to the elastic peak ($P=1.4$ eV) versus sample angle for W(110) + oxide at 300 K. $\Delta\theta_{\mathrm{FWHM}}$ is measured to be 10°.

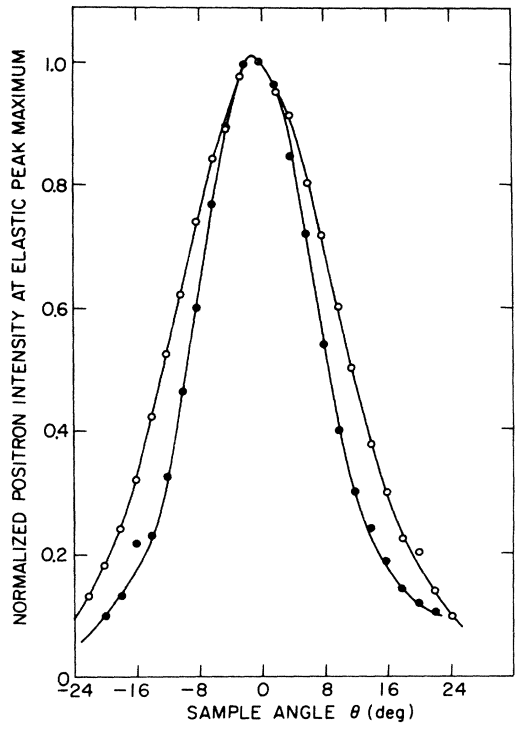

FIG. 9. Peak normalized positron intensity at the elastic peak maximum ($P=1.4$ eV) versus sample angle for clean Cu(111). Solid circles (●) for sample temperature of 23 K, $\Delta\theta_{\mathrm{FWHM}}=18°$. Open circles (○) for sample temperature of 300 K, $\Delta\theta_{\mathrm{FWHM}}=24°$. There is an observed narrowing of the positron-emission angle as the temperature is lowered.

the surface. This conclusion is strengthened by the systematically large range of ϕ^+ (0.4—4.1 eV) over which there is good agreement with calculations. At 23 K the Cu(111) distribution is significantly narrowed from the 300-K data. It is not, however, as narrow as expected from thermal broadening alone. Although this may be an indication of incomplete thermalization this angular width may instead have been broadened by surface steps or twinning that appeared in LEED observations of our Cu(111) crystal. It should also be noted that the low emission energy of Cu ($\phi^+=0.4$ eV) renders it the most susceptible to stray residual magnetic and electric fields which could broaden the angular distribution.

The data in Figs. 8 and 9 can also be used to set a crude upper limit on the fraction of positrons undergoing wide-angle *elastic* scattering that is in disagreement with theoretical predictions.[29] All previous measurements[1,2] of positron-reemission energy spectra were sensitive only to the component of energy ($E_z-P_z^2/2m$) parallel to the magnetic guiding field of the beam. Thus wide-angle

TABLE II. Comparison of the calculated and measured angular widths are summarized. The calculated width is based on thermal broadening of the positron's emission angle as per Eq. (9). The effect of ϕ^+, pass energy, analyzer angular resolution, and electric field distortion are accounted for as described in the text. The top three results are for 300 K while the bottom one is for 23 K.

Sample (ϕ^+ in eV)	$\theta_{1/2}$ [Eq. (9)]	θ_{FWHM}(calc)	θ_{FWHM}(expt)
W(110) + O (4.1±0.2)	5.6±0.1	12.7±1.2	10±1
W(11) + C (2.95±0.1)	6.2±0.1	13.9±1.2	13±1
Cu(111) (0.4±0.1)	9.9±0.4	24.2±1.0	24±1
Cu(111) at 23 K (0.4±0.1)	2.7±0.1	10.2±1.5	18±1

elastically scattered positrons could not be distinguished from inelastic events. Assuming that there is a uniform background of 0.02 in Fig. 8 that extends no further than $\pm 60°$, we estimate that the ratio of scattered to unscattered elastic events, R, must be less than unity. This is based on the solid angle of acceptance of the analyzer aperture being only 0.6% of 2π steradians when $P=1.4$ eV and that, when set to 0°, the analyzer accepts about $\frac{2}{3}$ of the unscattered elastic events. More reasonably, we might assume a $\cos\theta$ distribution for the elastically scattered positrons yielding $R<0.50$. Furthermore, a small fraction of the events attributed to scattered positrons in Fig. 8 may be background noise counts in the analyzer channeltron detector. Thus we conclude that in order for the elastic scattering intensity to be as much as 50% of the peak intensity [for W(110) + O] it must be distributed over a very wide angular distribution, or so strongly peaked about $\theta=0°$ so as to be indistinguishable from the thermally-broadened elastic peak. At the 10% level there is no significant low angle ($\theta=15°$–$20°$) elastic scattering by inspection of Fig. 8.

We conclude that the elastic peak distribution in energy and angle (after allowance is made for the assumed nonthermal tailing on the energy-gain side of the elastic peak) is consistent with thermal broadening at room temperature for all of the samples studied. At 23 K our lack of precise knowledge of the analyzer's energy and angular resolution (as well as our inability to increase the implantation energy beyond 3 keV) prevents us from rigorously testing the quantitative predictions of thermal broadening. We certainly can limit T_{eff}/T to be less than ≈ 4.

IV. DISCRETE POSITRON ENERGY-LOSS PROCESSES AT THE SURFACE

The reemission spectrum of positrons from a clean metal single crystal consists of an elastic peak, as discussed in the preceding section, and a broad, relatively structureless, inelastic continuum which extends down to the work-function cutoff (to be discussed in Sec. V). We consider here discrete energy-loss processes (i.e., vibrational excitations) that occur when adsorbed molecules are present on the reemission surface. The first observation of such discrete loss peaks in a positron-reemission energy spectrum was reported earlier in a Letter.[8] We begin with that experiment in which CO was adsorbed on Ni(100) and compare the results with the well-established results[30] from electron-energy-loss spectroscopy (EELS). The observed scattering cross sections will then be compared with an EELS dipole scattering theory with simple modifications to convert it to REPELS. The results of a new experiment to investigate nondipole (impact) scattering of reemitted positrons from NiO(111) + H_2O will then be presented.

CO was adsorbed at room temperature on the clean Ni(100) surface at a pressure of 2×10^{-8} torr. The characteristic $c(2\times2)$CO structure was observed (visually) with LEED to reach a maximum intensity at about 2 L exposure.[30,21] There is some uncertainty in the CO coverage due to residual H_2 gas in our ultrahigh-vacuum (UHV) surface chamber which results in a small equilibrium H_2 coverage on the Ni(100) surface. This coverage is dependent on the sample temperature and the partial pressure of H_2 as described in Ref. 31. For the CO on Ni(100) data presented here the residual H_2 pressure measured by a residual gas analyzer was less than 10^{-9} torr, which, from Ref. 31, puts the equilibrium H_2 coverage at less than $\frac{1}{8}$ of a monolayer. The surface H_2 limits the resulting CO coverage after exposure to $\frac{3}{8}$ of a monolayer.

Figure 10 shows reemitted energy spectra in the vicinity of the elastic peak for Ni(100). The expanded scales emphasize the energy-loss side of this peak in order to compare clean Ni(100) with Ni(100)$c(2\times2)$/CO. The energy-loss peak at 248 ± 10 meV for CO on Ni(100) appears as a shoulder on the tail of the elastic peak and is of similar width to the elastic peak. This agrees with 256.5 meV as measured by Andersson for CO on Ni(100) using EELS.[30] The relative loss intensity was found by taking the ratio of the loss peak to elastic peak height after background subtraction and was found to be $\approx 0.4\%$. The ratio was not sensitive to the particular method of background subtraction.

If we assume the dipole scattering mechanism applies to this loss process, the relative intensity is given by[32–34]

$$\frac{I_1}{I_0}=\frac{4\pi me^2}{\hbar^2 E_0}|\mu_1|^2\frac{n_s}{\cos\alpha}f(E_0,\alpha)\ . \tag{10}$$

where m is the electron mass, E_0 is the primary energy (which in this case is ϕ^+, as measured from the total reemitted-positron energy spectrum), μ_1 is the dipole matrix element between vibrational states 0 and 1, n_s is the number of molecules per unit surface area, and α is the angle of incidence. The quantity $f(E_0,\alpha)$ is a geometrical factor[34] given by

$$f(E_0,\alpha)=(\sin^2\alpha-2\cos^2\alpha)Y+(\sin^2\alpha+2\cos^2\alpha)\ln X\ ,$$

where α is the angle of the incidence with respect to the surface normal and

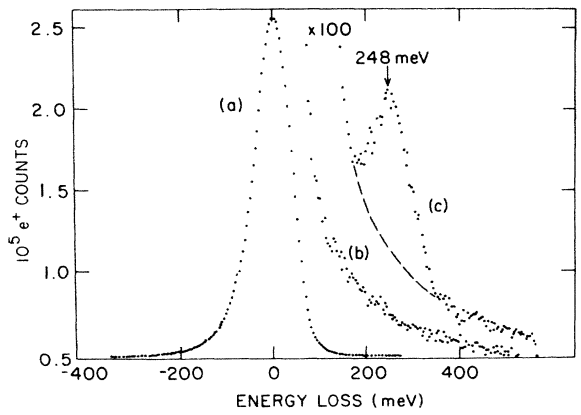

FIG. 10. Curve a, raw data for the elastic peak of clean Ni(100). Curves b and c show an expanded scale (times 100) of the reemitted-positron energy-loss spectra for clean Ni(100) and Ni(100)$c(2\times2)$/CO at 298 K. The C-O vibrational energy-loss peak is indicated by an arrow at 248 meV. The data shown are the result of a run 10 hours long. The count rate at the elastic peaks was approximately 5 kcps.

$$Y=\frac{\theta_1^2}{\theta_1^2+\theta_0^2}\ ,\quad X=1+\theta_1^2/\theta_0^2\ .$$

Here $\theta_0=\hbar\omega/2E_0$ (the angular deviation from the specular direction for a vibrational energy-loss scattering event) and θ_1 is the analyzer acceptance cone half-angle.

Applying these expressions to this REPELS experiment, we take $\alpha=0$, $E_0=\phi^+[\mathrm{Ni}(100)c(2\times2)/\mathrm{CO}]=1.6$ eV,[35] $n_s=8.06\times10^{18}$ molecules/m^2, $\theta_1\approx8°$, and $\theta_0\simeq4°$ (for $\hbar\omega=250$ meV). In this early experiment our analyzer half-angle of acceptance was 8° (not 5°), and hence nearly full collection of the loss peak intensity is possible since the loss-peak-intensity lobe is only 4° away from specular scattering. The dipole matrix element μ_1 in Eq. (10) has the form $\langle\psi_0\,|\,qX\,|\,\psi_1\rangle$, where q is the dynamic effective charge (dipole derivative $\partial\mu/\partial x$) and X is the rms displacement of the molecular harmonic oscillator from its ground state given by[33,34] $[\hbar/(2M_r\omega)]^{1/2}$, where M_r is the reduced mass. The matrix element μ_1 has (for electrons) been obtained experimentally by EELS to be $[(4.09\pm0.08)\times10^{-2}]ea_0$.[34] We can then calculate the expected relative loss intensity for the first vibrational state of CO using the EELS dipole scattering theory with our experimental parameters to be $I_1/I_0\approx1\times10^{-2}$. However, we must include an additional multiplicative factor of $\frac{1}{4}$ since the reemitted positrons traverse the CO molecule only once, whereas in an EELS experiment the electrons have two chances to interact, approaching and departing the surface (the scattering cross section is proportional to the square of the scattering amplitude). Therefore our measurement of the relative loss intensity, 0.4%, is in reasonable agreement with our estimate of 0.25%. No other significant difference between positrons and electrons is expected in the intensity ratio for dipole scattering since this is a long-range interaction (≈50 Å).[33]

All of the above calculations have been done by assuming incoherent scattering so that a total scattering intensity is merely equal to the scattering intensity from a single molecule times the total number of molecules. Different results would, in principle, be obtained for the coherent scattering case which involves summing the individual scattering amplitudes and squaring the result to obtain the total scattered intensity. However, for this system the results would be nearly identical because the CO molecules are weakly interacting.[36]

Our data have demonstrated the existence of vibrational energy-loss features in the reemitted-positron energy spectrum. In considering this technique as a complementary spectroscopy to EELS, we note that REPELS has some fundamental differences from EELS in that the sample itself provides the source of positrons. It is interesting to note that EELS cannot look in the forward scattering direction for specular reflection. Also, for short-range energy-loss processes (impact theory)[36] REPELS would allow the exclusion of the exchange interaction in cross-section calculations, thus simplifying the calculation.

In an effort to investigate the possibility of nondipole vibrational losses to surface molecules, we attempted to repeat the EELS experiments of Andersson and Davenport for OH adsorbed on a Ni(100) + oxide surface[34] with our REPELS apparatus. Andersson and Davenport found the energy dependence for the scattering intensity of OH to be much greater than could be explained by the dipole theory. This type of scattering is often referred to as impact scattering in order to differentiate it from the simpler dipole scattering mechanism discussed earlier.

We were not able to duplicate the NiO(111) surface described by Andersson; instead we obtained a NiO surface similar to that observed in Ref. 37. An initially clean Ni(100) was exposed to 300 L of O_2 at room temperature and subsequently annealed to 500°C. LEED revealed a $c(2\times2)$ oxygen pattern and the NiO(100) as described in Ref. 37. A REPELS spectrum revealed a positron work function (ϕ^+) change of $+0.45$ eV from the clean Ni(100) ϕ^+ of -1.4 to -0.95 eV for the Ni oxide which compares well to the electron work-function reduction of ≈0.3 V.[37] Deposition of OH onto the Ni-oxide surface was carried out by admitting a vapor of triply distilled, degassed water onto the cold (≈23 K) sample surface. Two exposures were performed, one with 2 L of H_2O and a second with 10 L, each monitored using a residual gas analyzer. A REPELS spectrum for each exposure was made. Three loss peaks for the H_2O-covered Ni-oxide surface were found at ≈110, ≈220, and ≈400 meV. We also noticed that the intensity of these peaks grows with OH-gas exposure. For the first exposure of 2 L, we believe this corresponds to a monolayer coverage of H_2O and consequently a five-monolayer coverage at 10 L exposure.[38] The LEED pattern of the underlying Ni-oxide is visible for a 2-L exposure, but no discernible pattern is visible for the 10-L exposure in general agreement with Ref. 38, an EELS experiment for Ni(100) + H_2O. The observed energy-loss peaks may be assigned physical meaning by assuming that at greater than one monolayer coverage the vibrational loss spectrum should resemble the infrared spectrum of ice[38,39] as shown in Table III.

The ratio of the 400-meV loss peak to the elastic peak intensity was found to be 1.3% and 3.7% for the 2-L and 10-L H_2O exposures, respectively. These ratios were found not to be sensitive to the particular method of background subtraction. Relative loss intensities for the 110- and 220-meV peaks were not calculated.

Utilizing the previously mentioned dipole scattering theory [Eq. (10)], we may calculate the expected I_1/I_0 for our analyzer geometry with $E_0=0.7$ eV (ϕ^+ as measured during the REPELS run) and the maximum dipole matrix element for the O-H stretch suggested by Ref. 34 is $\mu_1=3.73\times10^{-2}ea_0$. The intensity ratio for the O-H stretch was calculated using the dipole theory [Eq. (10)] to be $I_1/I_0=1.6\times10^{-3}$ (0.16%) for the one-monolayer exposure. Again the relative loss intensity must be modified by $\frac{1}{4}$ for positrons, as mentioned previously for the CO loss intensity calculation. Thus I_1/I_0 becomes 0.04%, which differs from the observed intensity by a factor of 32 and almost 100 for the five-monolayer case. From these results it is clear that positrons must have strong nondipole scattering at the surface similar to the electron-impact loss processes described in Refs. 34 and 38.

Figure 11 shows the relative loss intensity (I_1/I_0) versus primary electron energy for NiO(111) + OH from Ref. 34. The observed relative loss intensity,

TABLE III. The observed energy-loss peaks at their physical assignments (Refs. 38 and 39).

Energy-loss peak	Assignment
110 meV	H_2O "rotation"
220 meV	H bonding; "scissor-type" bending vibration of H_2O
400 meV	O-H stretch (for H bonding)

$I_1/I_0=1.3\%$ from the REPELS data on $NiO + H_2O$ (one monolayer), has been placed on this figure utilizing the measured positron work function of 0.7 eV as the primary energy. In addition, a hand-drawn line (dashed) through the data points has been added to indicate the general trend of the relative loss intensity. From this figure we see again that the dipole theory is an inadequate explanation for the observed results and in fact has the reverse energy dependence. By going to lower primary beam energy the scattering intensity seems to increase rapidly for this impact energy-loss process. REPELS can easily provide good intensities at low (<1 eV) incident energies, whereas in EELS going to low energy results in a severe restriction on the intensity output of the monochromator.

V. CONTINUOUS POSITRON ENERGY-LOSS PROCESS AT THE SURFACE

We have already discussed in Sec. IV discrete energy loss to the vibrational modes of adsorbed molecules. We will now address one process that produces a continuous energy-loss spectrum: electron-hole pair excitation and phonon production by the escaping positron. A smooth tail is observed in the REPELS spectrum extending from the elastic peak down to the zero energy, motivating the idea of continuous energy-loss processes at the surface. After the initial implantation the freely diffusing thermalized positron carries a correlation cloud of conduction electrons with it as it approaches the surface from the bulk. The correlation cloud and bare positron can be thought of as a "dressed" positron; that is, a positron diffusing in the bulk surrounded by a cloud of virtual electron-hole pairs[40] and which exists in a gas of phonons. The possible fates of a dressed positron as it crosses the surface region[40] are the following: elastic positron reemission with kinetic energy equal to ϕ^+; the inelastic reemission of the positron leaving a single electron-hole pair behind (multiple loss processes are clearly possible as well as phonon losses); and the elastic emission of positronium at the surface, which requires the removal of an electron from the metal leaving a hole behind. The formation of positronium is energetically possible if its work function, $\phi_{Ps}=\phi^+ + \phi^- - 6.8$ eV, is negative. Here 6.8 eV is the Ps ground-state binding energy. The "elastic" positronium thus formed is emitted with a kinetic energy of $-\phi_{Ps}$.

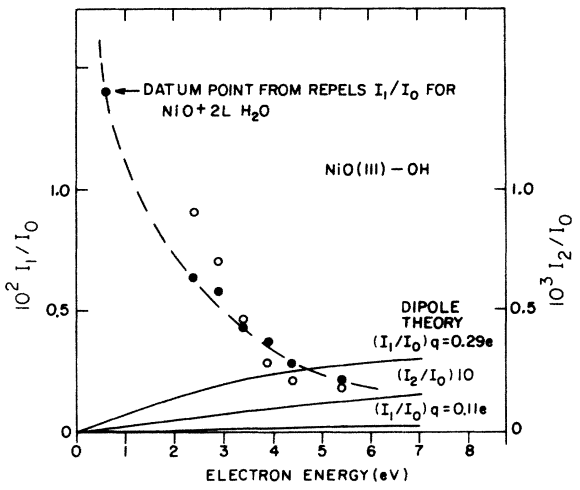

FIG. 11. Relative loss intensity versus primary electron energy for NiO(111)-OH derived from measured fundamental (●) and overtone (○) loss spectra. Solid curves are dipole predictions as explained in the text. The above figure is from Ref. 34. An additional datum point from the REPELS experiment of $NiO + H_2O$ (see text) has been added to the original figure. Also, a hand-drawn line through the data has been added to indicate the upward trend of the data at low input energy.

We wish to find an analytic expression for the observed inelastic tail assuming as a first approximation that the positron loses energy only through single electron-hole production upon reemission at the surface and that a phase-space estimate is sufficient. This corresponds to calculating the phase-space probability of observing a reemitted positron with energy E or equivalently with energy loss $E_L=\phi^+-E$. If $E_L>\phi^+$ the positron cannot escape into the vacuum and therefore cannot be counted in the analyzer, thus $E_L>\phi^+$ will not be considered here. From Fig. 12 we see that the number of available initial electron-hole states $[N_i(E_L)]$ corresponding to an energy loss E_L is the sum of the surface density of electronic states $[D_s(\epsilon)]$ from the Fermi energy (ϵ_F) down to an energy equal to E_L. Hence

$$N_i(E_L)=\int_{\epsilon_F-E_L}^{\epsilon_F} D_s(\epsilon)d\epsilon \ . \tag{11}$$

We may assume that the surface density of electronic states $D_s(\epsilon)$ is a constant, D, over the limits of integration (e.g., for copper E_L is at most 0.5 eV, $\epsilon_F=7$ eV,[41] and thus $E_L \ll \epsilon_F$). Then N_i becomes

$$N_i=DE_L \ .$$

The density of final reemitted-positron states $[D^+(\epsilon)]$ corresponding to an energy loss E_L [i.e., $D^+(E_L)$] is for free positrons reemitted into the vacuum proportional to p^2dp, a hemispherical shell in phase space with positron momentum p equal to $[(\phi^+-E_L)/2m_e]^{1/2}$. Assuming a constant matrix element, we find the probability of observing a reemitted positron that has lost energy E_L is

$$P(E_L)dE_L \propto E_L(\phi^+-E_L)^{1/2}dE_L \ . \tag{12}$$

We note that this is the same expression calculated by Pendry in Ref. 42.

Although Eq. (12) is a phase-space estimate for the rel-

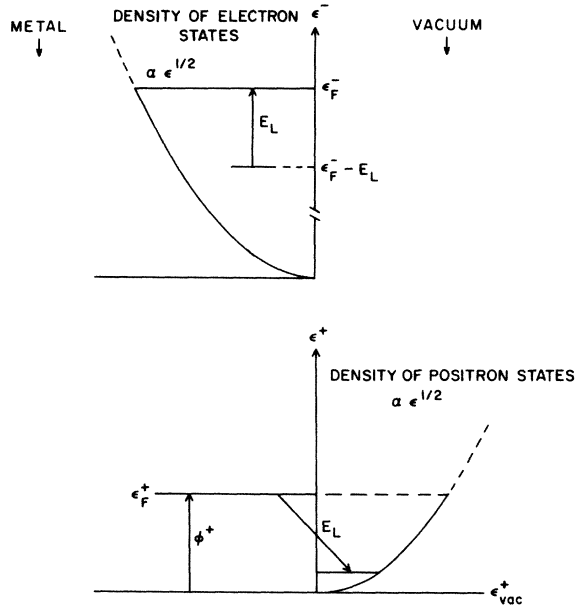

FIG. 12. Density of electronic states available for an energy loss E_L in electron-hole creation for a reemitted positron is shown in the upper diagram. Electronic states from energy $\epsilon_F^- - E_L$ to ϵ_F^- are available for excitation during the emission process. Also shown is the density of final states for a free positron (vacuum) which has undergone an energy loss E_L.

ative probability of producing a reemitted positron which has undergone an energy loss E_L, it must be further modified by the analyzer's angular acceptance efficiency as a function of E_L, i.e., $A(E_L)$ the fraction of the reemitted positrons (kinetic energy equals $\phi^+ - E_L$) accepted by the analyzer. $A(E_L)$ is given by the ratio of the analyzer angular acceptance α to the emission angle of a positron of initial kinetic energy $\phi^+ - E_L$ whose parallel energy component is $E_{||}$ (after the scattering event) and undergoes a subsequent perpendicular acceleration to make its total kinetic energy equal to the analyzer pass energy (see Sec. II):

$$A(E_L) \propto \frac{\alpha}{(E_{||}/P)^{1/2}} \propto \frac{1}{(E_{||})^{1/2}} . \tag{13}$$

The relationship between $E_{||}$ and E_L is not strictly known. As a first guess we assume that the positron-impact electron-hole production is a single Coulomb scattering event. The scattering angle θ is then given by simple kinematics:

$$E_L = E_{\text{incident}} \sin^2\theta = \phi^+ \sin^2\theta . \tag{14}$$

The angle of positron emission (θ) after the scattering event is given by

$$\sin^2\theta = \frac{E_{||}}{\phi^+ - E_L} . \tag{15}$$

Solving Eqs. (14) and (15) for $E_{||}$ gives

$$E_{||} = (\phi^+ - E_L)\frac{E_L}{\phi^+} . \tag{16}$$

Finally, the predicted intensity of reemitted positrons transmitted by the analyzer that have undergone a single scattering event of energy loss E_L to an electron-hole pair is given by the product of the analyzer collection efficiency $A(E_L)$ and the probability of the scattering event occurring $P(E_L)$ [using Eqs. (12), (13), and (16)]:

$$I(E_L)dE \propto (E_L)^{1/2} dE_L . \tag{17}$$

In Fig. 13 we have plotted the function $P(E_L)$ and the predicted intensity $I(E_L)$ which is area normalized to $P(E_L)$ over the range $0 \le E_L \le \phi^+$. This normalization was chosen to keep the total number of reemitted positrons the same for both functions.

In light of the simple density-of-states probability arguments given (which assumes no energy dependence for the transition matrix), we see from Fig. 13 that the calculated intensity $I(E_L)$ begins at zero for zero energy loss, reaches a maximum, and returns to zero at energy loss equal to ϕ^+. Since the elastic peak ($E_L = 0$) has a finite width due to thermal broadening and the analyzer resolution function also adds to this width, the actual observed intensity of reemitted positrons would not be expected to fall to zero at zero energy loss. However, from Fig. 13 we can at least conclude that we might observe a continuous distribution in energy of the reemitted positrons from the elastic peak down to zero kinetic energy for $E_L = \phi^+$. In fact, such a tail is observed in all of the REPELS spectra. Figure 14 shows a typical REPELS spectrum for W(110) plus an ordered carbon overlayer (the vertical scale has been expanded by a factor of 50). An energy-loss tail is clearly visible, extending from the elastic peak down to a cutoff at zero kinetic energy or $E_L = \phi^+$.

A more sophisticated theoretical study[43] of the inelastic tail incorporating energy dependence in the electron-hole pair production matrix element yields a large $P(E_L)$ at small E_L, similar to the data in Fig. 14. In this regard Mills[44] has speculated that the loss and gain side of the elastic peak may be asymmetrically broadened in much the same way that photoemission lines are broadened by

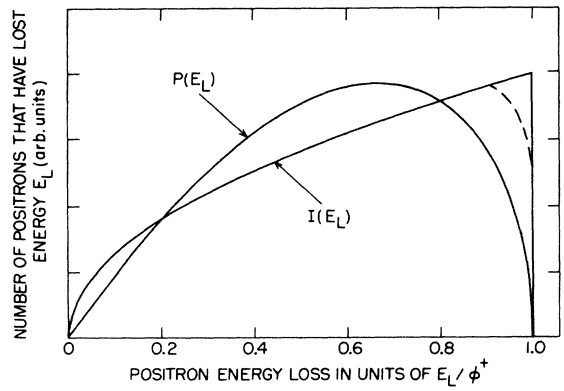

FIG. 13. Phase-space calculation of the relative probability, $P(E_L)$, of positrons that have lost energy E_L in the creation of an electron-hole pair upon reemission. Also shown is $P(E_L)$ corrected for the analyzer acceptance, $I(E_L)$, calculated assuming Coulomb scattering at the surface. The areas under each curve have been normalized. The dashed curve shows the effect of finite analyzer resolution.

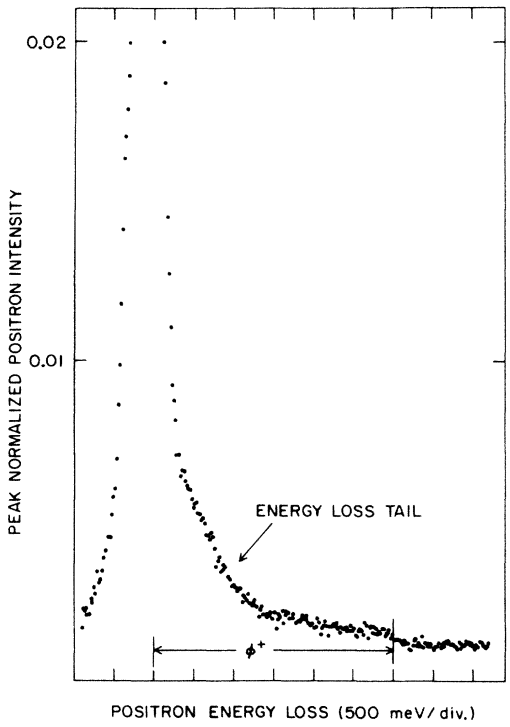

FIG. 14. Peak normalized (peak equals 1) reemitted-positron intensity versus positron energy loss for W(110) plus an ordered carbon overlayer. The positron work function ϕ^+ is shown and the energy-loss tail is indicated by an arrow ($P=1.4$ eV).

the singularity in electron-hole pair excitation at zero energy loss.[45] As pointed out in Sec. III, we do observe some additional broadening in the elastic peak beyond a beam Maxwell-Boltzmann distribution (see Fig. 7). However, the extreme conclusion of Neilson *et al.*,[43] that effectively all positrons emitted from a surface must proceed through an inelastic channel (and hence that the "elastic peak" is simply a manifestation of the singularity in electron-hole pair excitation at zero energy loss) is totally contradicted by a *clear elastic peak* that appears in all our data at 300 and 23 K for each sample. Indeed, the sudden appearance of a photoelectron hole and its attendant "shake-up" screening processes may not be analogous to the more gradual relaxation of the electron correlation cloud during positron emission. Positron excitation of electron-hole pairs on traversing the surface may be more closely related to pair excitation by low-energy electrons in EELS. In this case 2.3-eV electrons are known[46] to reflect off metal surfaces with an elastic peak of width 3 meV and with inelastic peak-normalized intensities less than 1% at all energies. Our inelastic continuum spectra are in qualitative agreement with those predicted in Ref. 46 for EELS. For W(110) + C the area under the inelastic tail is 1% of the peak area (see Fig. 14). Given the solid angle of acceptance of the analyzer this could be due to an inelastic component of 40% of the peak intensity, but with an isotropic angular distribution at all values of E_L. More reasonably, we might assume that Eq. (14) describes the angular distribution and then the relative intensity is only 5%. Without further studies of the wings of the analyzer resolution function as well as the angular distribution of inelastic scattering, we can make no definitive statements concerning these low intensity processes.

Finally, we note an interesting feature in the REPELS spectrum that implies that the relative intensity of inelastic scattering depends on surface order. Adsorbing oxygen on Ni to produce a disordered gas overlayer shows an order of magnitude increase in the inelastic continuum. Figure 15 (curve *a*) is a REPELS spectrum for Ni(100) with 300 L of oxygen adsorbed at 150 °C and exhibits a large inelastic tail. Curve *b* is the same surface (same vertical scale as curve *a*) annealed to 300 °C for 1 min and shows a relatively small inelastic tail with respect to curve *a*. The initial surface after exposure to 300 L of O_2 showed very fuzzy LEED spots indicating poor surface order. However, after the brief annealing a sharp $c(2\times2)$ LEED pattern was observed that is characteristic of NiO.[31] The oxygen coverage was found to be nearly the same before and after the anneal using Auger electron spectroscopy. Although we do not at present fully understand the enhancement in energy loss taking place in curve *a*, we present the data to show that REPELS as a surface spectroscopy is very sensitive to surface order.

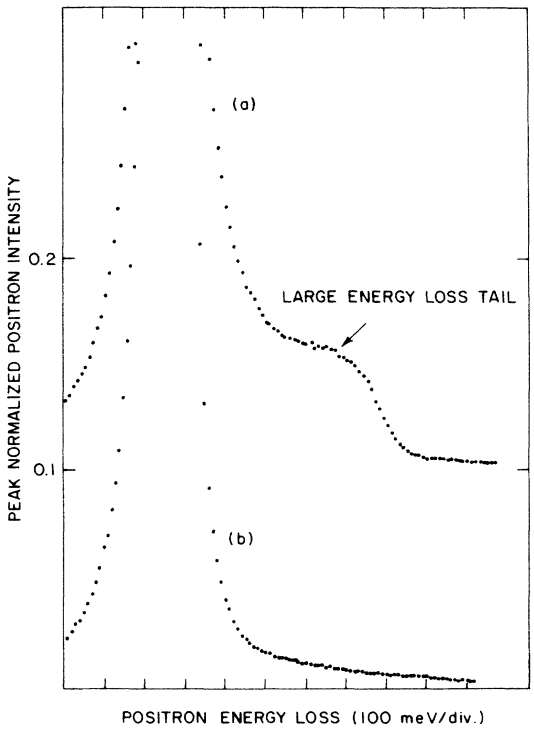

FIG. 15. Curve *a* shows the peak normalized (peak equals 1) reemitted-positron intensity versus positron energy loss for Ni(100) + 300 L of O_2 adsorbed at 150 °C (the curve has been displaced vertically by 0.1). A large energy-loss tail is observed as indicated by the arrow. Curve *b* shows the same as curve *a* but after annealing to 300 °C for 1 min. Note the large energy-loss tail is much reduced in intensity.

VI. CONCLUSION

In this paper we have presented the first total-energy, high-resolution ($\Delta E \approx 20$ meV) measurements of the reemitted-positron energy spectrum. Using an electrostatically focused positron beam and a hemispherical energy analyzer, we have observed a narrow elastic peak emitted along the sample normal with energy width and angular broadening governed by a beam Maxwell-Boltzmann distribution. At room temperature the measured energy width (FWHM) is ≈ 75 meV for Ni(100), Ni(100) + CO, Ni(100) + S, Ni(100) + O, W(110) + C, W(110) + Cu, W(100) + O, Cu(111), Cu(111) + S, and Cu(100) + S. The angular distribution of the elastically ($E = -\phi^+$) reemitted positrons at 300 K is consistent with thermal broadening for those samples investigated: W(110) + oxide ($\phi^+ = -4.1$ eV), W(110) + C ($\phi^+ = 2.95$ eV), and Cu(111) ($\phi^+ = 0.4$ eV). Such angular scans also showed that wide angle elastic scattering is at least 2 times less probable than direct elastic emission. A narrowing of the elastic peak energy width and angular spread is observed at 23 K. However, without improvement in analyzer resolution we can only rigorously conclude that the broadening is consistent with thermal positrons in the bulk for an effective temperature of $T_{\text{eff}}/T < 4$.

A continuous energy distribution of positrons is observed to extend from the elastic peak (kinetic energy equals $|\phi^+|$) down to the vacuum cutoff (zero kinetic energy) due to inelastic processes at the surface (i.e., electron-hole pair and phonon production). These processes are of low intensity (of order 10%) relative to the elastic peak, similar to such processes observed in EELS spectra.[46] With the results from the present study it is not possible to determine whether positrons or electrons have a higher inelastic scattering cross section at the surface. The inelastic scattering intensity is observed to increase with surface disorder (adsorbed O_2).

The first observation of discrete energy-loss peaks have been made in the reemitted-positron energy spectrum due to molecular vibrational excitations of adsorbed molecules on the sample surface as the positron traverses the surface during reemission. For Ni(100)$c(2\times2)$/CO at room temperature, energy-loss peaks were found at ≈ 57 and ≈ 248 meV, corresponding to the Ni-C and C-O stretching vibrations, respectively. The peak positions are consistent with previously reported EELS results and the intensity relative to the elastic peak is also consistent with the EELS long-range dipole scattering theory slightly modified for REPELS. The first evidence for short-range positron (impact) scattering in the case of OH on NiO was also observed in the 400-meV loss peak of the REPELS spectra.

In comparing REPELS and EELS the sample itself in REPELS is the source of monoenergetic positrons, whereas in EELS an electron monochromator is necessary in addition to the high-resolution analyzer. Thus in EELS if the monochromator and analyzer have the same resolution their resolutions add in quadrature, which gives a REPELS analyzer of similar resolution an intrinsic $\sqrt{2}$ energy resolution advantage over the EELS system. Also, off-specular scattering is easily accomplished in REPELS by simply rotating the sample in front of the analyzer. We have also shown that REPELS can easily provide good intensities at low (< 1 eV) incident energies, whereas presently, in EELS, going to low impact energy results in a severe restriction on the intensity output of the monochromator. At low (0.7 eV) primary beam energy the impact scattering intensity for OH on NiO was observed to be twice as large as the intensity observed for a similar EELS experiment (at 2.4-eV primary beam energy).

An improved REPELS system would utilize a brightness-enhanced electrostatically focused positron beam[47] in order to deliver a high positron flux through the narrow entrance slit of the REPELS analyzer. This will be important since a narrow REPELS analyzer slit is necessary in order to achieve a ($\Delta E/E < 0.1\%$) resolution approaching 1 meV. Then by maintaining the sample at or below liquid-He temperature (assuming the energy distribution is actually thermal even at 4 K), we would expect an energy resolution limited by that of the analyzer (≈ 3 meV is the best so far). Although a simple technique in principle, REPELS requires that the sample have a negative positron work function and be kept at low temperature in order to achieve adequate energy resolution. This restricts the experimenter in choice of sample and prevents the study of temperature-dependent effects. However, sample cooling is often used to "freeze" chemical reactions in a high-pressure gas-phase reaction chamber for subsequent translation to a UHV chamber containing EELS. One future solution is to change the REPELS experimental geometry to be similar to EELS, i.e., to use the reemission characteristics of a cold (< 1 K) moderator to produce a directed variable-impact energy beam of highly monoenergetic ($\Delta E < 1$ meV, assuming the reemitted spectrum remains thermal) positrons analogous to the electron monochromator of an EELS system. This simple positron "monochromator" could provide superior intensities and resolution to the complicated EELS monochromator which works poorly at low (< 1 eV) beam energies. Finally, spin-polarized positron beams[48] (which do not depolarize on thermalization) could be used to study spin-dependent processes (e.g., spin-dependent energy loss to molecules with unpaired spins).

ACKNOWLEDGMENTS

We thank W. E. Frieze, A. P. Mills, Jr., and J. Colbert for useful discussions. One of us (D.W.G.) thanks Brookhaven National Laboratory for its support and hospitality while visiting there. Work performed at Brookhaven is supported by the Division of Materials Sciences, U.S. Department of Energy, under Contract No. DE-AC02-76CH00016.

*Current address: National Synchrotron Light Source, Brookhaven National Laboratory, Upton, New York 11973.
[1]A. P. Mills, Jr., P. M. Platzman, and B. L. Brown, Phys. Rev. Lett. **41**, 1076 (1978).
[2]A. P. Mills, Jr., *Positron Solid-State Physics,* edited by W. Brandt and A. Dupasquier (North-Holland, Amsterdam, 1983), p. 432; K. G. Lynn, *ibid.*, p. 609.
[3]R. M. Nieminen and J. Oliva, Phys. Rev. B **22**, 2226 (1980).
[4]A. P. Mills, Jr., Phys. Rev. Lett. **41**, 1828 (1978).
[5]K. G. Lynn, Phys. Rev. Lett. **43**, 391 (1979); A. P. Mills, Jr., Solid State Commun. **34**, 623 (1979).
[6]D. W. Gidley, A. R. Köymen, and T. W. Capehart, Phys. Rev. Lett. **49**, 1779 (1982).
[7]R. L. Bell, *Negative Electron Affinity Devices* (Clarendon, Oxford, 1973).
[8]D. A. Fischer, K. G. Lynn, and W. Frieze, Phys. Rev. Lett. **50**, 1149 (1983).
[9]Peter J. Schultz, K. G. Lynn, W. E. Frieze, and A. Vehanen, Phys. Rev. B **27**, 6626 (1983).
[10]K. G. Lynn, Phys. Rev. Lett. **44**, 1330 (1980).
[11]D. A. Fischer, Ph.D. thesis, State University of New York at Stony Brook, 1984 (available from University Microfilms International, Ann Arbor, Michigan).
[12]K. D. Sevier, *Instrumental Methods of Electron Spectrometry and Methods of Electron Detection* (Wiley, New York, 1972).
[13]C. Kuyatt and J. Simpson, Rev. Sci. Instrum. **38**, 103 (1967)
[14]H. Hafner, J. Simpson, and C. Kuyatt, Rev. Sci. Instrum. **39**, 33 (1968).
[15]Purchased from Comstock, Inc. Oak Ridge, Tenn.
[16]Aerodag G purchased from Acheson Colloids Co., Port Huron, Mich.
[17]J. Parker and R. Warren, Rev. Sci. Instrum. **33**, 948 (1967).
[18]J. Hölzl and F. K. Schulte, in *Solid Surface Physics,* Vol. 85 of *Springer Tracts in Modern Physics,* edited by G. Höhler (Springer-Verlag, New York, 1979), p. 90.
[19]R. Poule, R. Lechey, J. Jenkins, and J. Liesegang, J. Phys. E **6**, 201 (1973).
[20]Lake Shore Cryogenics Inc., Westerville, Ohio.
[21]J. C. Tracy, J. Chem. Phys. **56**, 2736 (1972).
[22]J. E. Demuth and T. N. Rhodin, Surf. Sci. **45**, 249 (1974).
[23]G. E. Becker and H. D. Hagstrum, J. Vac. Sci. Technol. **11**, 285 (1974).
[24]A. M. Horgan and I. Dallins, J. Vac. Sci. Technol. **10**, 523 (1973).
[25]P. Kubica and A. T. Stewart, Phys. Rev. Lett. **34**, 852 (1975).
[26]C. A. Murray and A. P. Mills, Jr., Solid State Commun. **32**, 789 (1980); see also, Cherry A. Murray, Allen P. Mills, Jr., and J. E. Rowe, Surf. Sci. **100**, 647 (1980).
[27]P. Schrammen and J. Hölzl, Surf. Sci. **130**, 203 (1983).
[28]P. Kubica and A. T. Stewart, Can. J. Phys. **61**, 971 (1983).
[29]D. Nielson, R. M. Nieminen, and J. Szymanski (unpublished).
[30]S. Andersson, Solid State Commun. **21**, 75 (1977).
[31]K. Christmann, O. Schobu, G. Ertl, and M. Neuman, J. Chem. Phys. **60**, 4528 (1974).
[32]B. N. J. Persson, Solid State Commun. **24**, 573 (1977).
[33]S. Andersson, B. N. J. Persson, T. Gustafsson, and E. W. Plummer, Solid State Commun. **34**, 473 (1980).
[34]S. Andersson and J. W. Davenport, Solid State Commun. **28**, 677 (1978).
[35]D. A. Fischer and K. G. Lynn (unpublished).
[36]R. F. Willis, *Vibrational Spectroscopy of Adsorbates* (Springer-Verlag, Berlin, 1980).
[37]C. A. Papageorgoaoulos and J. M. Chen, Surf. Sci. **52**, 40 (1974).
[38]H. Ibach and S. Lehwald, Surf. Sci. **91**, 187 (1980).
[39]J. E. Bertie and E. Whalley, J. Chem. Phys. **40**, 1637 (1964).
[40]A. P. Mills, Jr., L. Pfeiffer, and P. M. Platzman, Phys. Rev. Lett. **51**, 1085 (1983).
[41]C. Kittle, *Introduction to Solid State Physics* (Wiley, New York, 1976), p. 154.
[42]J. B. Pendry, *Positron Solid State Physics,* Ref. 2.
[43]D. Neilson, R. M. Nieminen, and J. Szymanski, in Workshop on Slow Positrons in Surface Science, edited by J. W. Humberston and M. R. C. McDowell, Finland, 1984 (unpublished).
[44]A. P. Mills, Jr. (private communication).
[45]P. H. Citrin, G. K. Wertheim, and Y. Baer. Phys. Rev. B **16**, 4256 (1977).
[46]P. W. J. Persson and E. Zaremba, Phys. Rev. B **31**, 1863 (1985).
[47]W. E. Frieze, D. W. Gidley, and K. G. Lynn, Phys. Rev. B **31**, 5628 (1985).
[48]J. Van House and P. W. Zitzewitz, Phys. Rev. A **29**, 96 (1984), and references therein.